BIOCHEMISTRY
including biophysical chemistry & molecular biology
Article

Biochemistry **XXXX,** *XXX,* 000–000 A
DOI: 10.1021/bi9011989

Structural Insights into the Dual Activities of the Nerve Agent Degrading Organophosphate Anhydrolase/Prolidase[†]

Nand K. Vyas,[‡] Alexei Nickitenko,[‡,||] Vipin K. Rastogi,[§] Saumil S. Shah,[§] and Florante A. Quiocho*[,‡]

[‡]*Verna and Marrs McLean Department of Biochemistry and Molecular Biology, Baylor College of Medicine, Houston, Texas 77030 and* [§]*BioDefense Team, Research and Technology Directorate, U.S. Army-Edgewood Chemical Biological Center, Aberdeen Proving Ground, Maryland 21010.* [||] *Deceased.*

Received July 14, 2009; Revised Manuscript Received December 11, 2009

ABSTRACT: The organophosphate acid anhydrolase (OPAA) is a member of a class of bimetalloenzymes that hydrolyze a variety of toxic acetylcholinesterase-inhibiting organophosphorus compounds, including fluorine-containing chemical nerve agents. It also belongs to a family of prolidases, with significant activity against various Xaa-Pro dipeptides. Here we report the X-ray structure determination of the native OPAA (58 kDa mass) from *Alteromonas* sp. strain JD6.5 and its cocrystal with the inhibitor mipafox [*N*,*N*′-diisopropyldiamidofluorophosphate (DDFP)], a close analogue of the nerve agent organophosphate substrate diisopropyl fluorophosphate (DFP). The OPAA structure is composed of two domains, amino and carboxy domains, with the latter exhibiting a "pita bread" architecture and harboring the active site with the binuclear Mn^{2+} ions. The native OPAA structure revealed unexpectedly the presence of a well-defined nonproteinaceous density in the active site whose identity could not be definitively established but is suggestive of a bound glycolate, which is isosteric with a glycine (Xaa) product. All three glycolate oxygens coordinate the two Mn^{2+} atoms. DDFP or more likely its hydrolysis product, *N*,*N*′-diisopropyldiamidophosphate (DDP), is present in the cocrystal structure and bound by coordinating the binuclear metals and forming hydrogen bonds and nonpolar interactions with active site residues. An unusual common feature of the binding of the two ligands is the involvement of only one oxygen atom of the glycolate carboxylate and the product DDP tetrahedral phosphate in bridging the two Mn^{2+} ions. Both structures provide new understanding of ligand recognition and the prolidase and organophosphorus hydrolase catalytic activities of OPAA.

In the mid-1940s, the enzymatic nature of hydrolysis and detoxification of DFP in various tissues of rabbits and humans was explored (*1*, *2*). Twenty years later, Hoskins et al. identified two enzymes that detoxify organophosphorus compounds, such as DFP[1] [compound **I** (Scheme 1)] and soman (*3*). These enzymes are generally known as organophosphate/organophosphorus hydrolases (OPHs). Eventually, an organophosphorus acid anhydrolase (OPAA, EC 3.1.8.2) was purified from *Alteromonas* sp. strain JD6.5, a halophilic bacterial isolate, and shown to possess enzymatic activity against several highly toxic organophosphorus (OP) compounds such as the neurotoxic chemical warfare agents (CWA) DFP, sarin (**II**), soman, and tabun (*4*). OPAA exhibits high levels of hydrolysis activity against P−F bonds of the OPs, but very minimal activity for P−O and P−C bonds (*4*). Similar substrate specificity was later observed for the OPAA from *Alteromonas undina* (*5*) and *Alteromonas haloplanktis* (*6*). However, mipafox or DDFP, the close analogue of DFP, is not a substrate under normal assay conditions but a competitive inhibitor with a K_i of 0.49 mM for DFP substrate hydrolysis (*4*, *5*). OPPA is active at high pH (∼8.5) and requires divalent cations, typically Mn^{2+} (*4*−*6*).

OPAA has been considered as an important component in the development of an enzyme-based cocktail for decontamination of highly toxic OP-based CWA, including those listed above. Moreover, many pesticides used worldwide to protect crops and mammals are OP-based. Several insecticides are synthesized as "thion" (P═S bond) and activated by insect cytochrome P450 for conversion to the toxic "oxon" (P═O bond). (Interestingly, mammalian cytochromes convert thion-based insecticides less efficiently than bacterial and insect cytochromes.) This thion to oxon conversion of OP works as a safety feature for mammals when exposed to low levels of such insecticides (*7*). For practical purposes, detoxification of OPs by hydrolytic enzymes such as OPAA is an advantageous method for preventive self-decontamination and response decontamination (*7*−*9*).

Organophosphate-based CWA exert their main toxic effect through the phosphorylation of the active site serine residue of enzymes such as acetylcholinesterase (AChE) and neuropathy target esterase (NTE) of the central nervous system (*10*, *11*). Pharmacological studies have established the involvement of NTE in OP-induced delayed neuropathy in humans and in

[†]This work was supported by grants to F.A.Q. from the U.S. Army-Edgewood Chemical Biological Center and The Welch Foundation (Q-581).

*To whom correspondence should be adressed. E-mail: faq@bcm.tmc.edu.

[1]Abbreviations: AChE, acetylcholinesterase; AMPP or APPro, aminopeptidase P; CWA, chemical warfare agents; DFP, diisopropylfluorophosphate; mipafox or DDFP, *N*,*N*′-diisopropyldiamidofluorophosphate; DDP, *N*,*N*′-diisopropyldiamidophosphate; DMP, diisopropylmethylphosphonate; NTE, neuropathy target esterase; OP, organophosphorus/organophosphate/organophosphonate; OPAA, organophosphorus acid anhydrolase; OPH, organophosphate hydrolase; MetAP, methionine aminopeptidase; MAD, multiple-wavelength anomalous dispersion; PTE, phosphotriesterase; rmsd, root-mean-square deviation; SAD, single-wavelength anomalous dispersion.

Report Documentation Page

Form Approved
OMB No. 0704-0188

1. REPORT DATE	2. REPORT TYPE	3. DATES COVERED
11 DEC 2009		**00-00-2009 to 00-00-2009**

4. TITLE AND SUBTITLE	5a. CONTRACT NUMBER
Structural Insights into the Dual Activities of the Nerve Agent Degrading Organophosphate Anhydrolase/Prolidase	5b. GRANT NUMBER
	5c. PROGRAM ELEMENT NUMBER
6. AUTHOR(S)	5d. PROJECT NUMBER
	5e. TASK NUMBER
	5f. WORK UNIT NUMBER
7. PERFORMING ORGANIZATION NAME(S) AND ADDRESS(ES) **U.S. Army-Edgewood Chemical Biological Center,BioDefense Team, Research and Technology Directorate,Aberdeen Proving Ground,MD,21010**	8. PERFORMING ORGANIZATION REPORT NUMBER
9. SPONSORING/MONITORING AGENCY NAME(S) AND ADDRESS(ES)	10. SPONSOR/MONITOR'S ACRONYM(S)
	11. SPONSOR/MONITOR'S REPORT NUMBER(S)

12. DISTRIBUTION/AVAILABILITY STATEMENT
Approved for public release; distribution unlimited

13. SUPPLEMENTARY NOTES

14. ABSTRACT
see report

15. SUBJECT TERMS

16. SECURITY CLASSIFICATION OF:			17. LIMITATION OF ABSTRACT	18. NUMBER OF PAGES	19a. NAME OF RESPONSIBLE PERSON
a. REPORT **unclassified**	b. ABSTRACT **unclassified**	c. THIS PAGE **unclassified**	**Same as Report (SAR)**	**13**	

Scheme 1: Stereochemistry of OPAA Substrates (**I**, **II**, and **IV**), the Reaction Product (**III**), and the PTE Substrate Analogue (**V**)[a]

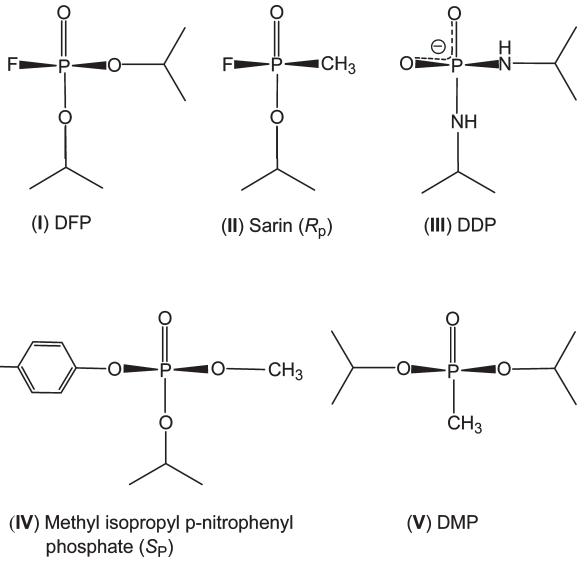

[a]To correlate with the stereochemistry of the ligands bound in the enzyme structures, the projection is patterned after the views shown in Figures 3A,C and 5 for DDP (**III**) bound to OPAA and DMP (**V**) bound to PTE as a common reference. See also the legend of Figure 5 for the description of the binding of DMP to PTE.

animal models (*12*). NTE, a 150 kDa transmembrane protein that has a serine esterase domain, is highly conserved from bacteria to mammals. Phosphorylation of the serine esterase domain by OPs, such as mipafox, leads to NTE inactivation (*13*). The mode of inhibition of AChE and NTE by OPs differs from that of OPAA. Whereas mipafox, like OPs, covalently attaches through phosphorylation of an active site serine residue of AChE and NTE, no similar adduct formation has been reported for DDFP-inhibited OPAA. Instead, mipafox or DDFP inhibition of OPAA is reversible and competitive against the substrate DFP (*4*, *5*).

Although the natural substrate of OPAA remains to be identified, it also possesses significant prolidase activity, with specificity for various dipeptides (Xaa-Pro) having proline as the second residue (*6*, *14*). The enzyme is not capable of hydrolyzing peptides of three amino acids with proline as the middle residue, indicating that it is indeed a Xaa-Pro dipeptidase (*6*, *14*). In addition, amino acid sequence alignment indicates structural and functional similarities of OPAA with other prolidases, including bacterial aminopeptidase P (named AMPP or APPro), proline dipeptidase, and prolidases (*6*, *14*, *15*). These proteins are evolutionarily related; all are bimetalloenzymes and break a peptide bond between Xaa and Pro in dipeptides or in the amino-terminal position of oligopeptides. Although AMPP also exhibits identical hydrolysis specificity, it prefers polypeptide substrates with the N-terminal Xaa-Pro dipeptide (*16*). Collagen, which is rich in proline and hydroxyproline, is digested by tissue and bacterial collagenase (during pathogenic invasion), and intracellular prolidase catalyzes the final step of collagen breakdown to liberate proline for recycling (*17*). In humans, prolidase deficiency caused by mutations in prolidase genes is linked to a rare metabolic disease characterized by mild to severe skin lesions. Patients with prolidase deficiency excrete massive amounts of imidodipeptides in urine (*17*).

In this paper, we report the crystal structure analysis of the native OPAA from *Alteromonas* sp. strain JD6.5 of a halophilic bacterial isolate and its cocrystal with the inhibitor mipafox. Results of this study led to the determination of the two-domain structure of the enzyme, one domain exhibiting the pita bread motif and harboring the active site; the molecular details of the active site, which contains a binuclear Mn^{2+} center; the unexpected revelation of a nonproteinaceous density in the active site, surmised to be a bound glycolate; the unraveling of the molecular nature of mipafox inhibitor binding; a fresh and illuminating comparison with the structures and activities of bacterial AMPP, primarily a prolidase but also capable of degrading OPs, and phosphotriesterase, a well-characterized OPH; and the uncovering of a common mechanism for bridging the two active site metal ions by products and inhibitors. The structures serve as a framework for protein engineering experiments for the improvement of the catalytic efficiency toward OP substrates and stability of OPAA for decontamination of G- and V-type chemical warfare agents and pesticides.

MATERIALS AND METHODS

OPAA Purification and Crystallization. OPAA was originally isolated and characterized from *Alteromonas* sp. strain JD6.5 (*4*) and later cloned and expressed in *Escherichia coli* (*14*). The procedures for overexpression and purification of OPAA used in this study follow essentially those described in a previous publication (*18*). They are described briefly in the Supporting Information. Enzyme preparations, which usually exhibit a purity of >90% (data not shown), are dialyzed extensively against 0.1 mM $MnCl_2$ and 10 mM Bis-Tris propane (pH 8).

Prior to crystallization, the purified OPAA was dialyzed against 1 mM β-mercaptoethanol, 0.1 mM $MnCl_2$, and 10 mM Tris-HCl (pH 7.2) and concentrated to 10 mg/mL. Crystals of the enzyme in the absence or presence of 1 mM mipafox or DDFP were obtained at 20 °C by the hanging drop method, with the reservoir filled with a solution of 16% PEG 4000, 20 mM $MnCl_2$, 1 mM β-mercaptoethanol, 270 mM ammonium acetate, and 60 mM sodium acetate (pH 4.6). A typical hanging drop consisted of 2 μL of the protein solution and 2 μL of the well solution. Crystals with dimensions of ~0.4 mm × ~0.05 mm × 0.05 mm were grown in 2−4 days. Prior to diffraction data collection, crystals were equilibrated in the reservoir solution and flash-frozen in a stream of nitrogen gas cooled at ~100 K.

Determination of the Structure of Native OPAA. As indicated in Table S1 of the Supporting Information, six different diffraction data sets were collected on the Howard Hughes Medical Institute beamline 8.2.1 at the Advanced Light Source, Lawrence Berkeley National Laboratory (Berkeley, CA). The beamline allowed measurements of anomalous dispersion data from Mn^{2+} (three different wavelengths) and Os (one wavelength). Since OPAA requires Mn^{2+} for enzyme activity (*4*, *5*), throughout the purification and crystallization of the OPAA high concentrations of $MnCl_2$ were always present (see also the methods of the Supporting Information). The single anomalous dispersion (SAD) data set was collected from a native crystal soaked in 1 mM K_2OsO_4. All diffraction data sets were processed and scaled using either MOSFLM or HKL2000 (*19*, *20*). The crystal properties and statistics of the data sets are listed in Table S1. The crystals of OPAA and its complex with mipafox are isomorphous, and the asymmetric unit contains three OPAA molecules with no evidence of a 3-fold noncrystallographic axis of symmetry.

Combined multiple-wavelength anomalous dispersion (MAD) data from the Mn^{2+} in the native OPAA crystal and SAD data of the osmate-soaked crystal were used to obtain initial experimental phases (Table S1). The positions of 16 Mn^{2+} atoms and 6 osmate molecules in the asymmetric unit were determined, heavy atom parameters refined (figure of merits listed in Table S1), and phases calculated to 3 Å resolution (native OPAA data set) using the suite of programs in CNS (*21*). The calculated electron density map was solvent flattened, NCS averaged, and phase extended to 2.5 Å resolution. The resulting 2.5 Å electron density map was used to fit ~80% of the 517-residue OPAA sequence (*14*) initially to one (molecule A) of the three independent molecules using O (*22*) and CHAIN (*23*). The A molecule model was then superposed on the electron density of the other two molecules. The model was refined in CNS interspersed with model building and inclusion of water molecules. Although NCS restraints were applied initially to all residues in the three OPAAs in the asymmetric unit, they were removed in the final rounds of refinement, which were performed at 2.3 Å resolution. The final structure refinement statistics are summarized in Table S1.

Determination of the Structure of OPAA Crystallized in the Presence of the Inhibitor Mipafox or DDFP. Using the one diffraction data set (Table S1), the structure of OPAA cocrystallized with DDFP was determined by molecular replacement using the coordinates of the native structure stripped of all nonprotein atoms and then refined to convergence at 2.7 Å. We later considered that the bound ligand is the reaction product DDP; hence, a second round of refinement was carried out wherein the F atom of DDFP was replaced with an O atom to make the conversion to DDP. For reasons described in Results and Discussion, we favor an interpretation in which DDP is the bound species.

Deposition of Coordinates and Structure Factors. The coordinates and structure factors for the native OPAA and its complex with DDP (Table S1) have been deposited in the Protein Data Bank (PDB) (entries 3L24 and 3L7G, respectively).

Software Programs and Packages. For structure refinement and analyses, we used the suites of programs in CNS (*21*). The DALI server, a network server (http://www.ebi.ac.uk/dali/), was used for comparing the OPAA structure with similar protein structures available in the PDB. The conformational accuracy of both OPAA structures was assessed by PROCHECK (*24*). MOLSCRIPT and LIGPLOT were used to create molecular figures (*25*, *26*).

OPAA Enzymatic Assays. To determine the effects of potential inhibitors or compounds on the enzymatic activities of OPAA, three different assays (described in the Supporting Information) using different substrates were performed. The substrates are DFP (Sigma-Aldrich), Gly-Pro (Sigma-Aldrich), and *p*-nitrophenyl soman (*O*-pinacolyl *p*-nitrophenyl methylphosphonate), and the potential inhibitors include acetate, glycine, and glycolate at concentrations of 10 mM. The OPAA preparation used in these assays was, as indicated above, extensively dialyzed against a buffer that contained no β-mercaptoethanol.

RESULTS

Structure Determination. The structure of the native OPAA was the first to be determined by combined MAD and SAD techniques (Table S1). The refined structure was then used to determine the structure of the isomorphous enzyme crystal obtained in the presence of mipafox or DDFP (see Materials and Methods). The same complex structure but with DDP (**III**) in place of DDFP was also refined, and for reasons discussed below, it is the structure described here. The structure of the native OPAA was refined at 2.3 Å resolution and that with bound DDP at 2.7 Å resolution to R_{work} values of 23.5 and 20.3% and R_{free} values of 27.3 and 26.0%, respectively, and good geometry (Table S1).

The OPAA structure consists of three molecules (identified as A, B, and C) in the asymmetric unit, with no local 3-fold rotation axis of symmetry in a self-rotation calculation and no significant and uniform total buried surfaces between pairs of them (from 810 $Å^2$ for the A-B pair to 490 $Å^2$ for the A-C pair). These buried surfaces are considerably lower (~3−5 times) than those observed for bona fide or obligate dimer or oligomer or crystal packing interfaces of nonspecific protein−protein contacts (*27*).

Since OPAA purified from three different bacterial sources (natural bacterial cells and recombinant forms) is apparently a monomer in solution (*4*−*6*), the finding of three independent molecules in the crystal structure has no structural or functional significance. The presence of three independent molecules is, however, most invaluable for providing a multiplicity of data for the analysis of the structure and function of OPAA that follows.

Our structure analysis has also revealed that Ala439 of the published sequence of the *Alteromonas* sp. strain JD6.5 OPAA (*14*) is a leucine residue (see results and Figure S1 of the Supporting Information).

OPAA Structure. Of the total 517 residues of OPAA from *Alteromonas* sp. strain JD6.5 (*14*), only the first 440 residues could be fitted to the electron density of the three independent molecules in the asymmetric unit of the two OPAA structures. The remaining invisible 77-residue segment could only be attributed to high flexibility, since two independent mass spectrometric measurements, one for the dissolved crystals and another for the purified enzyme, indicated a mass consistent with the full-length protein (data not shown). In the crystal structures, there is a space close to the last observed residue in all three independent molecules that could possibly accommodate the last unresolved 77 residues. Coincidentally, the amino acid sequences of OPAA from *A. haloplanktis* consist of only 440 amino acids, being ~80% identical to the sequence of the first 440-residue segment of the *Alteromonas* sp. strain JD6.5 enzyme (*6*). OPAA from *A. undica* also has a mass very similar to the mass of that from *A. haloplanktis* (*5*, *6*). Deletion of the last 77 residues of OPAA caused no effect on enzyme activity (data not shown). Another much shorter disordered segment occurs in approximately similar locations in the three structures, residues 351−365 in molecule A (Figure 1A,B), residues 346−368 in molecule B, and residues 346−368 in molecule C.

The OPAA structure is composed of two domains (Figure 1A, B), a small N-terminal domain or N-domain (from residue 1 to ~160) and a large C-terminal domain or C-domain (residues ~161−440). Although both domains of OPAA consist of mixed β-sheets with an almost equal number of β-strands (six and five in the N- and C-domains, respectively), they differ in overall topology and shape. In the β-sheet of the N-domain, the central pair of strands (1 and 2) is antiparallel, while the flanking pairs of strands (3 and 4, and 5 and 6) are parallel. In contrast, all five β-sheet strands (7−11) in the C-domain are antiparallel. The β-sheet in the N-domain is twisted, whereas that in the C-domain is strongly curved, much like a "pita bread" first ascribed to the

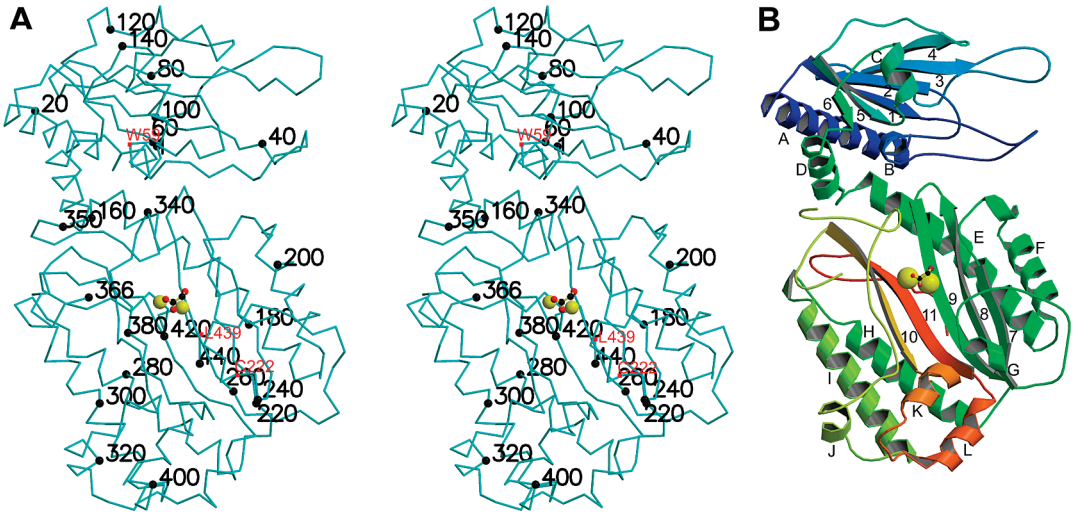

FIGURE 1: OPAA structure. (A) Stereo diagram of the Cα backbone trace of the native OPAA (molecule A). With the exception of three residues, every 20th Cα atom is marked by a solid black sphere and the residue number. The two Mn^{2+} atoms are shown as yellow spheres, and the bound putative glycolate is depicted as a ball-and-stick model. The color scheme for atoms used in this and all other figures for OPAA is as follows: yellow for Mn^{2+}, black for C, blue for N, and red for O. The locations of residues W59, C222, and L439 are identified with red Cα spheres and residue labels. W59 and C222 are the tryptophan and cysteine residues closest to the bimetallic center. Residues 351−365 are invisible or disordered. (B) Ribbon backbone trace color ramped from the N- to C-terminal ends. The α-helices are identified with letters, and the β-sheet strands are numbered.

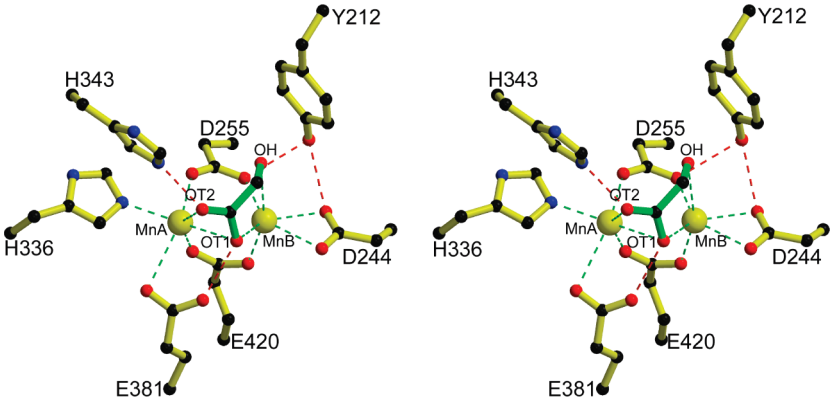

FIGURE 2: Stereoview of the binuclear Mn^{2+} center and the bound putative glycolate molecule. Ball-and-stick model of OPAA active site residues (yellow bonds) that are involved in the coordination of the two metal ions (yellow spheres) and in the interaction with the glycolate molecule (green bonds). Metal coordinations are shown as green dashed lines, while hydrogen bonds and other contacts with the glycolate are shown as red dashed lines. Note that the hydroxyl group of Tyr212 makes a bifurcated hydrogen bonds with the carboxylate side chains of Asp244 and Asp255.

architecture of a similar domain in the *E. coli* methionine aminopeptidase (MetAP) structure (*28*). The contents and topological arrangements of α-helices in the two domains also differ. The N-domain contains four helices, one pair (A and B) flanking one side of the β-sheet and the second pair (C and D) contacting the other side. In contrast, the pita bread C-domain contains almost 2 times more helices, with four long helices, arranged topologically in the order FEHI, fronting one face (the outer convex) of the β-sheet. The three remaining, relatively shorter helices (JKL) form a cluster on the outermost part of the domain, near the N-terminus of helix I. The C-domain harbors the catalytic center, located in an oval shallow cavity on the concave surface of the highly curved β-sheet.

Binuclear Mn^{2+} Cluster and a Nonproteinaceous Density in the Active Site of Native OPAA Structure. The two Mn^{2+} atoms [identified as MnA and MnB (Figure 2 and Figure S2A of the Supporting Information)] are separated by 3.3 ± 0.1 Å (average of distances in the three independent molecules). This demonstration of the presence of the two metal ions not only provides the most conclusive direct evidence of the observation of metal cation requirement for OPAA activity but also establishes the location of the catalytic center (Figure 1A,B). It is noteworthy that MnA is more solvent-exposed while MnB is more buried.

As shown in Figure 2 and Table 1, eight side chain O and N atoms from five residues (Asp244, Asp255, His336, Glu381, and Glu420) deployed by different β-sheet strands of the C-domain are engaged in coordination of the two Mn^{2+} ions. One metal atom (MnA) is coordinated by a monodentate carboxylate group (Glu381) and His336. The other metal (MnB) is ligated by a bidentatate carboxylate group of Asp244. On the other hand, both carboxylate oxygens of Asp255 and Glu420 act as nearly symmetrical bidentate bridges between the two metal cations. Interestingly, all the oxygens of the carboxylate side chains coordinate the Mn^{2+} ions in the more favorable *syn* configuration (*29*).

The structures of ligand-free enzymes with binuclear metal active sites usually show a hydroxide ion or water molecule bridging the two metal cations (*30*). However, a bridging hydroxide or water is not present in the active site of the native OPAA structure. Electron density maps generated using experimental

Table 1: Coordination Distances of the Binuclear Mn^{2+} in the OPAA Structures with Bound Putative Glycolate and DDP[a]

OPAA and glycolate atom	Mn_A^{2+} (MnA)[b]	Mn_B^{2+} (MnB)[b]	OPAA and DDP atom	Mn_A^{2+} (MnA)[b]	Mn_B^{2+} (MnB)[b]
Asp244 OD1		2.4 (0.1)	Asp244 OD1		2.3 (0.1)
Asp244 OD2		2.4 (0.1)	Asp244 OD2		2.4 (0.0)
Asp255 OD1		2.0 (0.0)	Asp255 OD1		2.1 (0.1)
Asp255 OD2	2.0 (0.1)		Asp255 OD2	2.1 (0.1)	
His336 NE2	2.4 (0.1)		His336 NE2	2.2 (0.1)	
Glu381 OE2	2.2 (0.2)		Glu381 OE2	2.1 (0.1)	
Glu420 OE1		2.3 (0.0)	Glu420 OE1		2.1 (0.1)
Glu420 OE2	2.2 (0.1)		Glu420 OE2	2.1 (0.1)	
glycolate OT1	2.5 (0.1)[c]	2.1 (0.1)	DDP O1	1.8 (0.1)	2.2 (0.1)
glycolate OT2	2.6 (0.1)[c]		DDP O2	3.2 (0.1)[c]	
glycolate OH		2.6 (0.1)[c]	DDP N1		2.9 (0.1)[c]

[a]Average of values from the three independent OPAA molecules. [b]The A and B designations of the two Mn^{2+} metals in OPAA were patterned after those in AMPP structures (e.g., see ref *38*). This was prompted by the finding that OPAA and AMPP have very similar structures (discussed in the text). [c]The coordinating distance is relatively longer than those formed with ligating residues. A recent survey of distances around metal sites in high-resolution ($\leq$1.25 Å) protein structures indicated that the coordination distances of Mn^{2+} with the same two sets of atoms of carboxylate O and His N have means of 2.12 and 2.16 Å, respectively, but distances of 2.5 Å or even up to 3.0 Å are not uncommon (*51*).

phases and throughout the course of structure refinement showed consistently a well-defined density that is much larger and more elongated than what would be expected for a more spherical bridging hydroxide or water molecule. The portion of the density closest to the two metal cations displays two bifurcated bulges. Since OPAA crystals were obtained in the presence of acetate and then finally equilibrated in a reservoir solution containing a much greater concentration of acetate [270 mM ammonium acetate and 60 mM sodium acetate (pH 4.6)], we assumed initially that the density represented an acetate molecule. This assumption was reinforced by a previous finding of a bound acetate [from a 50 mM acetate buffer (pH 4.6)] in the bimetallic center of the structure of *E. coli* aminopeptidase P (AMPP) (*31*), a proline aminopeptidase that is considerably similar in structure and function to OPAA (further discussed below). Although an acetate model fits easily into the extraneous density, with its carboxylate oxygens occupying the two bulges closest to the two metal cations, we noticed the presence of an "extra" density contiguous to the methyl group of the acetate. Following a series of structure refinements, which included the acetate molecule, an $F_o - F_c$ difference electron density map calculated without omitting the acetate confirmed the existence of the extra density (Figure S2A). This finding clearly indicates a bound ligand other than acetate. Moreover, a high concentration (10 mM) of acetate does not inhibit the hydrolysis of three different substrates (DFP, Gly-Pro, and *p*-nitrophenyl soman) by an extensively dialyzed OPAA (Table S2 and methods of the Supporting Information). For unknown reasons, acetate apparently stimulates enzyme activities toward DFP and *p*-nitrophenyl soman substrates.

Our initial speculation about the nature of the extra density was predicated on (1) the chemical features of the area closest to the extra density, which are contributed mainly by MnB, the carboxylate side chain of the metal ligating Asp255, and the aromatic side chain of Tyr212, and (2) the possibility that the site occupied by the entire elongated density represents the binding site (or S_1 site) for the N-terminal Xaa (or P_1) residue of the Xaa-Pro (P_1-P_2') dipeptide substrates or reaction product (further discussed below). These factors are suggestive of a polar group such as an amino or ammonium group for the extra density, implying a bound glycine (Xaa). A fitted glycine molecule refined well, and its density resolved well (data not shown). However, a high concentration (10 mM) of glycine does not inhibit the hydrolysis of DFP or *p*-nitrophenol soman substrates (Table S2).

Continuing with the assumption of a polar group, we found the extra density could also represent a hydroxyl group, which would suggest a bound glycolate molecule. As to be expected, the modeled glycolate refined just as well (Figure S2A), with its OH group coinciding with the α-amino group of the initially fitted and refined glycine molecule. A bound glycolate is also suggested by the finding that a glycolate concentration of 10 mM inhibits OPAA activities toward all three substrates [~50% inhibition for DFP and Gly-Pro substrates and ~30% for *p*-nitrophenyl soman substrate (Table S2)]. However, given that complete inhibition was not achieved by the high concentration of glycolate, the identity of the nonproteinaceous density is far from certain. Other compounds, such as β-mercaptoethanol, a component of the crystallization buffer solution, and ethylene glycol, a potential contaminant of the PEG 4000 precipitant (see Materials and Methods), were also considered but were deemed unlikely to represent the nonproteinaceous density for structural and biochemical reasons (described in the Supporting Information). We are therefore going on the assumption of a bound glycolate, which is isosteric with and in many ways behaves like glycine.

All three glycolate oxygens are involved in a tripartite coordination of the bimetallic cations (Figure 2 and Table 1). Acting in a bidentate manner, the carboxylate OT1 atom bridges the two metals and OT2 ligates MnA. The OH hydroxyl group contacts MnB at a distance somewhat longer than the coordination distances involving side chain oxygen and nitrogen atoms (Table 1) . The glycolate further interacts with active site residues (Figure 2 and Table S3 of the Supporting Information), of which two are worth noting. An intriguing interaction is between the carboxylate OT1 atom and the Glu381 OE1 atom, which can occur only between a negatively charged carboxylate and a protonated carboxyl group. The involvement of the carboxylate OT2 atom in coordinating MnA and hydrogen bonding His343 and the OT1 atom in bridging the two Mn^{2+} metals favors an ionized carboxylate group of glycolate. This implies that the protonated carboxylic acid belongs to Glu381 rather than to glycolate. The predisposition of the Glu381 to a protonated carboxyl group may have a bearing on the catalytic mechanism of prolidase (discussed below). Another interesting observation is that, besides making a long contact with MnB, the glycolate OH group engages in an OH$-\pi$ interaction (*32*) with Tyr212 (Figure 2 and Table S3). The Tyr or Phe residue is highly conserved in several prolidases (*15*), although this is, to the best

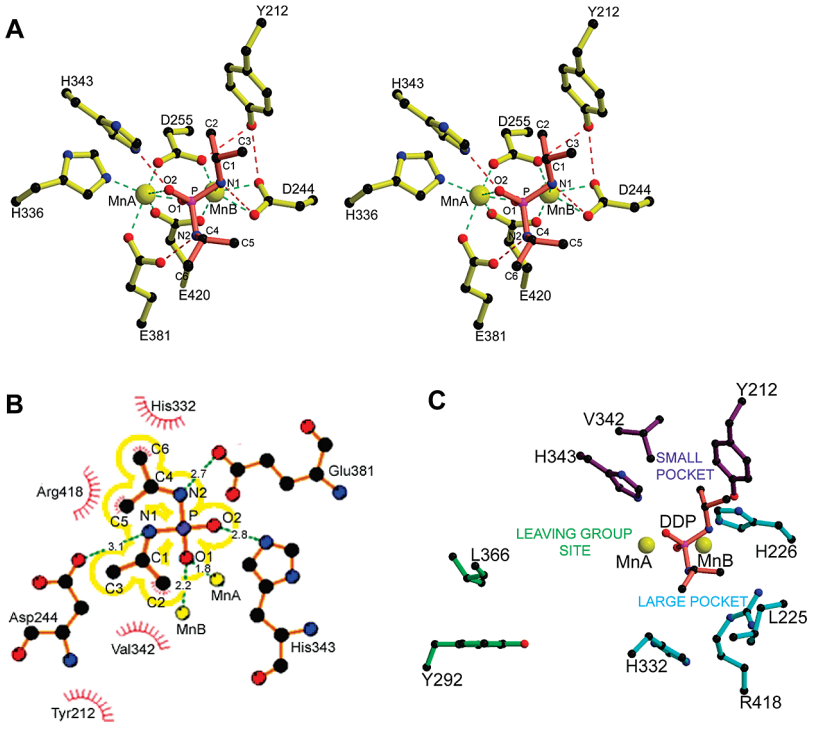

FIGURE 3: Binding of the reaction product DDP (**III**). (A) Stereoview of the ball-and-stick model of the OPAA active site, showing the coordination of the two Mn^{2+} ions, both with distorted octahedral geometry, and the electrostatic interactions associated with DDP (salmon bonds) (see also Tables 1 and S3). For MnA, His336 NE2, Glu420 OE2, and DDP O1 and O2 are nearly in plane and Glu381 OE2 and Asp255 OD2 are axial ligands. For MnB, Asp244 (OD1 and OD2), Asp255 OD1, and DDP O1 are nearly in plane and Glu420 OE1 and DDP N1 are axial ligands. (B) Ligplot of interactions between DDP (circumscribed by a yellow boundary) and OPAA via hydrogen bonds (dashed green lines) and nonpolar interactions with residues demarcated by a spoked arc. (C) Approximate locations of the small and large pockets and the so-called "leaving group site". Same view as in panel A.

of our knowledge, the first instance in which the interaction has been noted in a prolidase.

Including the contacts made by glycolate OT1, OT2, and OH atoms, the ligands surrounding both Mn^{2+} ions adopt a six-coordinate distorted octahedral geometry (Figure 2). Ligands His336 NE2, Glu420 OE2, and glycolate OT1 and OT2 are roughly in plane with MnA, and ligands Asp255 OD2 and Glu381 OE2 are axial ligands. For MnB, ligands Asp244 (OD1 and OD2), Asp255 OD1, and glycolate OT1 are approximately in plane, while those of Glu420 OE1 and glycolate OH are axial ligands.

Structure of the Complex of OPAA with Mipafox (DDFP) or Its Hydrolysis Product, DDP (***III***). To gain an understanding, at the atomic level, of the mode of inhibition by mipafox, we determined the structure of native OPAA crystallized in the presence of the inhibitor. Although the structure with the bound mipafox or DDFP was logically the first to be analyzed, another more realistic alternative of a bound hydrolysis or reaction product, DDP, was also investigated. Since the equivalent F and O atoms differ by only one electron, distinguishing between DDFP and DDP is impossible, especially at 2.7 Å resolution. However, we argue in favor of a bound DDP, produced under crystallization conditions (see Discussion), and the OPPA−product complex is the subject of the report that follows.

The difference electron density of the bound DDP is shown in Figure S2B. The structure of OPAA in complex with DDP is indistinguishable from that with glycolate; the rmsd of the superimposed α-carbon atoms of both structures (A molecules only) is 0.2 Å. The Mn−Mn distance is 3.4 ± 0.1 Å (the average from the three independent molecules). As observed in the OPAA−glycolate complex structure, both Mn^{2+} metals are completely devoid of ligated hydroxide or water molecules.

The coordination of the binuclear Mn^{2+} cluster by side chain atoms is also identical to that in the OPAA−glycolate complex structure (Figures 2 and 3A and Table 1). Moreover, the involvement of the O1 and O2 atoms of the tetrahedral phosphate and N1 atom in a tripartite ligation of the two metal cations is equivalent to the involvement of the OT1, OT2, and OH atoms, respectively, of glycolate. The O1 atom engages as an unsymmetrical bridging atom between the two Mn^{2+} metal ions. The lone pairs of O2 and N1 have relatively longer coordinating distances to MnA and MnB, respectively. Like those for the bound glycolate structure, both metals in the DDP-bound structure also show a six-coordinate distorted octahedral geometry (Figure 3A).

Besides coordinating the two metals, DDP interacts with OPAA residues via electrostatic interactions through its N1 and N2 and O2 atoms and nonpolar interactions primarily by way of its two isopropyl moieties, which occupy unique positions in the active site (Figure 3B,C and Table S3). The N1 and N2 atoms donate hydrogen bonds to Asp244 OD2 and Glu381 OE1, respectively, which are also metal ligand residues. The O2 atom accepts a hydrogen bond from the His343 NE, which is also mimicked by glycolate OT2 (Table S3). The two isopropyl groups are engaged in different hydrophobic interactions, the one a more buried C2−C1−C3 group with Tyr212 and Val342 and the other a more exposed C5−C4−C6 group with nonpolar atoms of His332 and Arg418 (Figure 3B,C). Interestingly, with the exception of the C5−C4−C6 isopropyl group, a majority of the interactions associated with DDP binding occur at the site of glycolate binding (Figures 2 and 3A,C and Table S3).

The DDP-bound structure has revealed three sites near the bimetallic center for interacting with the ligand, small and large pockets and the leaving group site (Figure 3C). Tyr212 and Val342 (Figure 3A,B) combine with His343 to form a small pocket which harbors the C2−C1−C3 isopropyl group. A larger pocket formed by Leu225, His226, His332, and Arg418 contains the C5−C4−C6 isopropyl group. The phosphoryl O2 atom is directed toward the leaving group site.

DISCUSSION

DDP or DDFP and DFP. There are two experimental conditions for preferential binding of DDFP as an inhibitor or DDP as a product. Under standard enzyme assay conditions with DFP as the substrate, which are very similar to those described in the methods of the Supporting Information, DDFP has been shown to inhibit OPAA from *Alteromonas* sp. strain JD6.5 and *A. undina*, with an identical K_i value of ~0.5 mM (*4*, *5*). Under the same conditions, DDFP (1 or 3 mM) is barely hydrolyzed by the enzyme (< 1% of the activity of DFP) (*4*, *5*), thereby favoring it as an inhibitor. DDFP was also shown in the mid-1980s to inhibit similar enzymes from *E. coli* and hog kidney (*3*, *33*). With no active site serine residue present, the binding of DDFP to OPAA clearly differs from that to acetylcholinesterase and neuropathy target esterase, which is accomplished by covalent attachment through phosphorylation of an active site serine residue (*10*, *13*).

The second set of conditions, which ultimately formed the basis of the structure analysis of the cocrystal, has the reaction product DDP bound. Although DDFP is a very poor substrate, it is, under the crystallization conditions, hydrolyzed by OPAA crystals or by enzyme in solution to yield a more than sufficient amount of DDP for complex formation. With l mM DDFP and 85 μM OPAA in the crystallization drop, which is an enzyme concentration ~4 orders of magnitude greater than that in the normal DFP assay (1.5×10^{-3} μM), and crystallization for ~3 days, complete DDFP hydrolysis is possible, even though the enzyme activity in solution at the pH (4.6) of crystallization is estimated to be ~5% of that at the optimum pH of ~8 (*4*). In an assay measurement at pH 4.6, monitored by the release of fluoride and mimicking the cocrystallization conditions (1 mM DDFP and 5 mg/mL OPAA), DDFP is hydrolyzed at an initial rate of ~500 nmol/min. The same measurement at pH 8.5 is too fast to follow. Since hydrolysis of DDFP in aqueous solution has a half-life of ~200 days (*34*), it is unlikely the source of DDP. There is a precedent for product formation and binding as revealed in the crystallographic studies of AMPP with an active site His361Ala mutation; despite the low activity of the mutated enzyme (< 1% of that of the wild type) in solution, the structure of the crystal of the mutant soaked for 1 h in a solution containing a Val-Pro-Leu peptide substrate showed the binding of the product Pro-Leu dipeptide at the active site, in a manner very similar to that seen in the native AMPP−Pro-Leu complex structure (*35*) (discussed further below).

Our structural studies provide a molecular basis for the binding of DDP and, by inference, DDFP under the conditions described above. On the basis of the DDP binding geometry (Figure 3A,B), we conclude that metal bridging O1 atom originates from the attacking hydroxide or water molecule and the O2 atom corresponds to the phosphoryl oxygen of DDFP. As discussed below, the O1 atom nearly coincides with the hydroxide ion or water molecule bridging the two metal ions in native AMPP. DDFP would bind in the inhibitory mode with its phosphoryl F and oxygen atoms occupying the positions of the O2 and O1 atoms, respectively, of DDP. The coordinating and other electrostatic interactions, combined with the hydrophobic interactions, govern the binding of DDP. As shown in panels A and B of Figure 3 and Table S3, the two NH groups (N1 and N2) of DDP (and also DDFP) donate hydrogen bonds to the side chains of Asp244 and Glu381, respectively. These specific charge-neutral hydrogen bonds are unlikely to be duplicated by DFP since both have oxygen atoms in place of the nitrogens of DDFP or DDP. This presumably makes DFP a far better substrate.

Questions of Whether the Active Site Contains Cysteine Residues and Whether DFP Binding Causes Major Structural Changes. Two independent studies showed that OPAA apparently requires a sulfhydryl group for catalysis (*4*, *5*). Moreover, it has also been demonstrated that OPAA apparently undergoes large changes in circular dichroism upon addition of the DFP substrate (*36*). Reducing agents (e.g., β-mercaptoethanol and dithiothreitol) stimulate OPAA activity, whereas thiol-specific reagents, such as *p*-chloromercuribenzoate, iodoacetate, and *N*-ethylmaleimide, inactivate OPAA against the DFP substrate (*4*). The two OPAA structures, which were obtained from proteins crystallized in the presence of β-mercaptoethanol (see Materials and Methods), provide no explanations for how reducing agents enhance or thiol-specific compounds abrogate OPAA activity. OPAA contains five Cys residues (residue 68 in the N-domain and residues 167, 222, 298, and 368 in the C-domain), all of which are in the reduced form and nowhere close to the binuclear Mn^{2+} ions (distances ranging from ~13 to 30 Å). Moreover, no pair of cysteines in the structure comes remotely close to forming disulfide bonds. Cys222, which is buried in the short α-helix G in the C-domain, is closest to the active site (Figure 1A). These observations indicate that if cysteines have to play a role in catalysis, it is accomplished indirectly and over considerable distances via an unknown mechanism. As discussed below, the prevailing proposed catalytic mechanisms of prolidase and OPH activities do not require the participation of a cysteine residue.

CD measurements indicated that DFP binding to OPAA causes both a significant reduction in the α-helical content and a considerable increase in the β-strand composition (*36*). These findings of major substrate-induced structural changes are difficult to reconcile given a compact and stable "supersecondary structure" (the packing of the α-helices and β-strands) of both domains (Figure 1A,B). Moreover, a compact supersecondary structure, together with the observation that the only Trp residue (W405) in the C-domain is far (~29 Å) from the active site binuclear Mn^{2+} ions, makes the observation of a DFP-induced change in tryptophan fluorescence (*36*) also inexplicable. There are four other Trp residues (59, 69, 89, and 100), but they are all located in the N-domain at distances from the active site ranging from 24 to 39 Å. Extensive crystallographic studies of the binding of a variety of ligands, including substrates, products, and inhibitors, to the Mn^{2+}-loaded and -free AMPP, which has a structure similar to that of OPAA (discussed below), also show no extensive ligand-induced structural changes relative to the ligand-free structure (for examples, see refs (*37*−*39*)). Given all these observations, OPAA is unlikely to undergo large substrate-induced conformational changes.

OPAA and Aminopeptidase P (AMPP or APPro) Comparison: Substrate and Product Recognition and Prolidase/Peptidase Activity. Both OPAA and AMPP belong to the family of prolidase bimetalloenzymes, whose large C-terminal

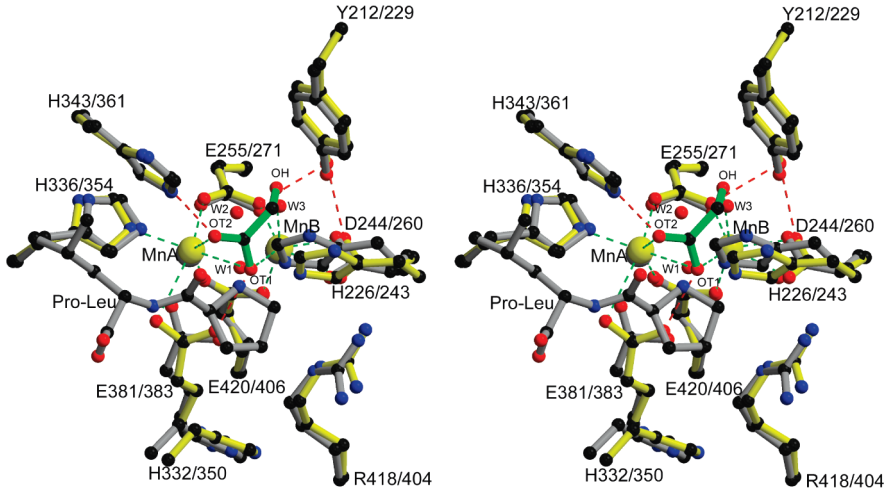

FIGURE 4: Stereoview of the superpimposed active sites in the pita bread domain structures of the complexes of OPAA with glycolate (green) and AMPP with the Pro-Leu dipeptide (gray). For the PDB entry of the AMPP structure, see Table S4. The OPAA residue identifications are first, followed by AMPP. Because the two Mn metal ions in both enzymes superimposed almost perfectly, the pair (gray spheres) in AMPP is obscured. W2 and W3 are water molecules linked to MnA and MnB, respectively, of AMPP, and their positions are close to those of OT2 and OH, respectively, of glycolate. Water molecules W1, W2, and W3 are also present in the native, ligand-free AMPP structure (Table S4).

domain exhibits a pita bread architecture. With several structures of complexes with ligands, combined with biochemical studies, AMPP is the best characterized of the family (*35* and references cited therein). The fact that the crystal structures of OPAA and AMPP, especially the active site-bearing C-terminal domains, are very similar allows a straightforward direct comparison between the two enzymes. For this, we superimposed the C-terminal domains of OPAA with bound glycolate and AMPP with bound C-terminal product Pro-Leu (P_1'-P_2'), which also contains a well-resolved bridging hydroxide molecule (*31*), or the inactive His254Ala mutant form of AMPP with bound Val-Pro-Leu (P_1-P_1'-P_2') substrate (*35*). The superpositioning resulted in a rmsd of ~2 Å for ~240 superimposed Cα positions and a 31% sequence identity. As further evidence of a very high degree of structural similarity, the active sites of both proteins, including the residues coordinating the binuclear Mn^{2+}, are composed of identical residues, which are superimposable (Figure 4; see also Table S4 of the Supporting Information). The two ligand-bound AMPP structures have delineated the subsites (S_1, S_1', and S_2') for binding the tripeptide substrate or dipeptide product. The glycolate occupies for the most part the S_1 subsite.

The superimposed active sites (Figure 4) provide further insight into the molecular features of peptide substrates or product recognition. Since the residues contacting the proline of the di- or tripeptide bound in AMPP are identical to those in OPAA, the features for P_1' Pro residue recognition are preserved in OPAA. The specificity of AMPP for the Pro residue is achieved mainly by van der Waals contacts of the hydrophobic atoms of His350 and Arg404 with the prolidyl ring (specifically, CB-CG and CG-CD atoms, respectively) (*35*, *39*). His350 and Arg404 of AMPP are equivalent to His332 and Arg418, respectively, of OPAA. Interestingly, the same hydrophobic atoms are also utilized in the interactions with one of the two isopropyl groups of DDP (described above with Figure 3).

The binding of glycolate has all the earmarks for recognition and binding of amino acid Xaa or the P_1 reaction product. Indeed, the glycine molecule was the first to be modeled to the nonproteinaceous density and successfully refined. The only difference is that the OH group of glycolate coordinated to the more buried MnB metal is the α-amino group of a Xaa residue of substrates or products. The amino group of the Val-Pro-Leu substrate has been observed to interact with the MnB in the inactive mutant AMPP (*35*). As mentioned above, the α-amino group could further participate in a NH−π interaction with the conserved Tyr [residue 212 in OPAA and residue 229 in AMPP (see Figure 2)], further contributing to substrate or product recognition. The carboxylate of the amino acid product would interact with the two metal ions and side chain residues in a manner exactly identical to that of the carboxylate of glycolate. Finally, it is interesting to note that the positions of the carboxylate OT2 and OH/NH_2 groups are close to those of the W2 and W3 water molecules associated with MnA and MnB, respectively, in the native AMPP (Figure 4). Expulsion of these water molecules by ligands [e.g., glycolate and DDP (Figures 2 and 3)] and the Val-Pro-Leu (P_1-P_1'-P_2') substrate bound to an inactive AMPP (*35*) contributes a favorable entropic effect to ligand binding.

From the overlapped OPAA and AMPP active sites, we observed that the two pockets and the leaving group site delineated in the binding of DDP to OPAA (Figure 3C) are also present in AMPP and involved in binding of the peptide substrate and product. The Pro-Leu product bound in AMPP occupies not only the leaving group site but also a portion of the large pocket. The aliphatic side chain of the N-terminal Val residue of the Val-Pro-Leu substrate bound to the inactive AMPP is directed toward the small hydrophobic pocket. This observation is fully consistent with the findings that the best prolidase substrates are ones in which the Xaa residues have large hydrophobic side chains (*4*−*6*). We note that the binding of the inhibitor apstatin to AMPP (*37*) makes extensive use of all three sites.

On the basis of extensive crystallographic and biochemical studies of AMPP, a catalytic mechanism for prolidase activity has been proposed and recently refined (*35*, *39*) (see Scheme 1 in ref *39*). Elaborations of some features of the mechanism based on our OPAA structures are as follows, with reference to Figures 2 and 4 and Tables 1 and S3. First, the bridging hydroxide or water molecule, which is clearly identified in the structure of AMPP with bound Pro-Leu, acts as the nucleophile by attacking the carbonyl carbon of the scissile peptide bond. The OT1 atom of the carboxylate of the glycolate bound in OPAA occupies almost

exactly the same position of the bridging solvent molecule (W1) in the native AMPP, suggesting the direction of the nucleophilic hydroxide attack of the Xaa carbonyl carbon of a Xaa-Pro substrate. Second, nucleophilic attack is facilitated by the polarization of the solvent molecule by binding to one or both metals and the abstraction of a proton by a general base, believed to be Glu383 in AMPP, which is equivalent to Glu381 in OPAA. OPAA Glu381 engages in hydrogen bonding with the bridging OH or OT1 atom of glycolate. Glu383 in AMPP and Glu381 in OPAA are also linked to the more solvent-exposed MnA ion. Third, the nucleophilic attack is further aided by polarization of the scissile peptide carbonyl bond through coordination with MnA and hydrogen bond formation with the NE2 group of His361 in AMPP. The glycolyate OT2 atom, which would mimic the peptide carbonyl oxygen, points toward His343, the equivalent of the AMPP His361, and MnA in ways envisioned for the Xaa carbonyl oxygen of the scissile bond of a substrate during catalysis. Fourth, the interactions of the scissile peptide carbonyl oxygen with a His residue (His361 in AMPP or His343 in OPAA) and MnA further stabilize the *gem*-diol intermediate that is formed following the nucleophilic attack. Moreover, every AMPP structure showed that the ND1 atom of His361 is in close contact with a carboxylate group of an Asp residue (Asp38) from an adjacent subunit, thereby resulting in a doubly protonated, positively charged imidazolium side chain of His361, which is believed to further enhance the formation of the *gem*-diol intermediate. In sharp contrast, however, this contact or charge coupling interaction is not present or even possible in OPAA since it does not have the counterpart of the Asp residue in AMPP. Moreover, unlike the homotetrameric AMPP (*31*), OPAA is, as indicated above, a monomer. Fifth, in the final step of peptide hydrolysis, collapse of the intermediate to products is facilitated by the donation of the abstracted proton from Glu383 in AMPP (equivalent to Glu381 in OPAA) to the amine of the Pro product. As suggested by the glycolate-bound structure (see above), the side chain of Glu381 appears to be predisposed to protonation. In the mechanism, the Xaa (P_1) amino acid product is bound in such a way that its carboxylate engages in a bidentate interactions, one oxygen bridging the two Mn^{2+} ion and the other coordinating only one metal ion, MnA, which is more exposed. These interactions are exactly those observed for the glycolate carboxylate (Figure 2), a surrogate of glycine.

Differences and Similarities of OPAA and Bacterial Phosphotriesterase (PTE): OPH Activity. Among the members of the large family of bimetalloaminohydrolases, the phosphotriesterase from *Pseudomonas diminuta* is the best characterized. Its structures in complexes with several OP substrate analogues, product and product analogues, and inhibitors have been determined, and the substrate and stereochemical requirements have been investigated extensively in solution [e.g., see a review article (*40*) and a recent paper (*41*)]. These studies have also generated a proposed catalytic mechanism for the hydrolysis of OP substrates (*40*−*42*).

With one exception, the substrates of PTE, such as organophosphonates [e.g., sarin (**II**) and soman and their analogues] and paraoxon (organophosphotriester) and its analogues (e.g., **IV**), are shared with OPAA (*43*, *44*). The one exception is that the nerve agent VX is hydrolyzed by PTE but is inert to OPAA (*18*). Both enzymes require bimetallic ions for activity, which are typically Zn^{2+} or Co^{2+} ions for PTE (*45*). Two features of the stereoselectivity in PTE were also later observed in OPAA: preferential hydrolysis of the least toxic R_p-enantiomers of organophosphonate sarin (**II**) and soman and their analogues and the S_p-enantionmers of organophosphate triesters (such as **IV**) (*43*, *44*). In PTE, substrate hydrolysis proceeds via the S_N2 mechanism with an inversion of the stereochemical configuration at the phosphorus center (*46*). As an OPH, AMPP exhibits the same mechanism, but interestingly, in contrast to OPAA, the hydrolysis of sarin analogues by the wild-type enzyme and binding site residue mutants prefers the S_p-enantiomers over the R_p-enantiomers (*47*). However, since two of the mutated binding site residues (Trp86 and Arg153) are contributed by or originate from another subunit of the tetrameric AMPP, they are naturally absent and thus have no bearing on the catalytic reaction of the monomeric OPAA.

Unfortunately, unlike AMPP, the fact that the quaternary and crystal structures of PTE and OPAA are completely different precludes a direct comparison between them. PTE is a dimer, whereas OPAA is a monomer. The PTE subunit, which is smaller (36 kDa), consists of one large domain which adopts a $(\beta/\alpha)_8$ or TIM barrel motif. In clear contrast, as described above, OPAA contains two distinct domains, with the largest, active site-bearing C-domain showing a highly curved β-sheet, akin to a pita bread (Figure 1). Moreover, both domains fold into mixed β-sheets, with the one in the N-domain flanked by helices on both sides and the other in the C-domain flanked by four helices on the outer surface. The active site in OPAA is located in a shallow cavity on the surface of the highly curved β-sheet, whereas that in PTE is situated in a pocket within one end of the barrel and surrounded mainly by $\beta-\alpha$ loops. Finally, as summarized in Table S4, the metal-coordinating residues and geometries differ between the two OPHs. One major difference is that the two metal ions in PTE require more His residues for coordination, whereas those in OPAA involve more acidic residues. Given these differences, a direct comparison of the active sites of the two enzymes is virtually impossible.

To be able to compare and contrast the bimetallic catalytic centers of OPAA and PTE and thereby make sound assessments of ligand binding and OPH catalysis, we came up with the following strategy: superposition of the pairs of divalent metals in the structures of the complexes of PTE with the substrate analogue diisopropylmethylphosphonate (DMP, **V**) (*48*) and OPAA with the DDP product (Figure 3A), together with the metal bridging OH hydroxide in PTE and the O1 atom of DDP and, crucially, impose the observations that MnA in OPAA and the so-called Znβ metal in PTE are more solvent exposed while MnB and Znα in OPAA and PTE, respectively, are more buried (see further Table S4 for the identifications of the metal ions). The outcome of the overlapped bimetallic centers, which is summarized in Table S5 and shown in Figure 5 for only the most important common features related to enzyme activity, is illuminating. Besides the overlapped pairs of metals (MnA and Znβ and MnB and Znα) and bridging atoms (rmsds of 0.3, 0.2, and 0.4 Å, respectively), seven side chain atoms coordinating the two metals in both enzymes superimposed with rmsds ranging from 0.3 to 1 Å. However, as expected, the overlapped side chain atoms are of mixed types: three between oxygens and nitrogens and four between oxygens. OPAA His336 and PTE His201 are the only two identical residues in both active sites that show the best overlap. The large and small pockets and the leaving group site that are close to the bimetallic center, which were brought to light by the structures of PTE in complex with substrate analogues and inhibitors (e.g., see refs *45* and *48*), approximately overlap in both enzymes OPAA and PTE. In both enzymes, the three sites have loose specificities.

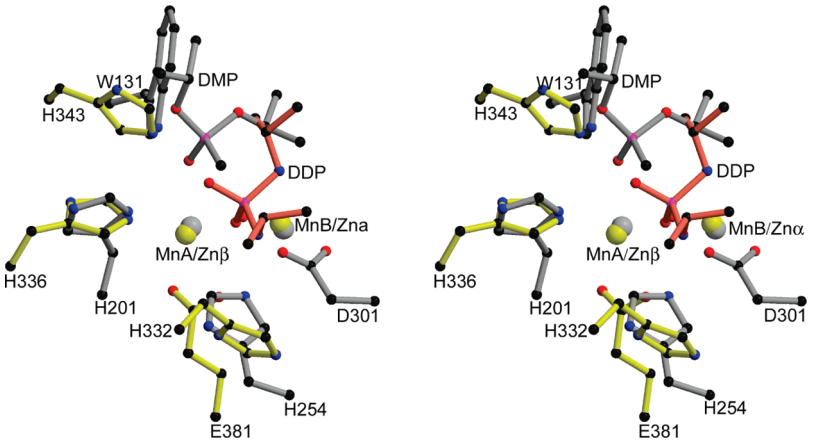

FIGURE 5: Stereo figure of the bound reaction product DDP (**III**) (salmon color) to OPAA and substrate analogue diisopropylmethylphosphonate [DMP (**V**), gray] to PTE. The orientation is almost identical to that shown in panels A and C of Figure 3, which also identifies the three sites (small and large pockets and leaving group site). The basis for overlaying of the active sites in OPAA and PTE, whose structures are completely different (pita bread and TIM barrel, respectively), is detailed in the text. Only few functionally relevant residues of the overlapped sites are displayed. Note that the NE2 atom of His343 overlaps with the NE1 atom of Trp131 of PTE. The nature of the coordination of the two metal ions in PTE is summarized in Table S4. The mode of binding of the DMP inhibitor is thought to resemble the binding of OP substrates to PTE (*48*). The phosphoryl oxygen docks on the more exposed Znβ metal ion; one of the isopropyl groups (situated to the "left" of the phosphorus center) occupies the leaving group site; the other isopropyl group resides in the small pocket; and the methyl group faces the large pocket.

Finally and more importantly, the comparison of the bimetallic centers of PTE and OPAA reveals that the features of the proposed catalytic mechanism for OP substrate hydrolysis by PTE (*41*, *42*) for the most part apply to OPAA or AMPP. Resembling the DMP binding to PTE (Figure 5), the phosphoryl oxygen of OPAA substrates (e.g., **I**, **II**, or **IV**) docks on the more exposed metal site, MnA in OPAA, which is equivalent to Znβ in PTE, and the leaving group F faces or the *p*-nitrophenyl resides in the leaving group site. Other phosphoryl substituents occupy approximately the small and large pockets [e.g., the methyl and isopropyl groups, respectively, of **II** and **IV** (see also Scheme 1 and Figures 3C and 5)]. [For DDFP to be acted upon as a substrate (under the conditions of crystallization described above), it will have to bind in the same productive manner, with its phosphoryl oxygen docking on MnA, at the position of the O2 atom of the bound DDP (Figures 3A).] It is also possible for the substrate phosphoryl oxygen to further form a hydrogen bond with the NE2 atom of His343 of OPAA (Figure 5), a residue that is highly conserved in other similar prolidases (*15*), including His361 in AMPP (Figure 4). We note that the role of the NE2 of His343 as a hydrogen bond donor group could be played by the NE1 atom of Trp131 of PTE (Figure 5). These combined interactions polarize the phosphoryl oxygen bond and enhance the electrophilicity of the phosphorus center. Similar interactions and functions have been proposed for the carbonyl oxygen of the scissile peptide bond of peptide substrates of AMPP (*39*), which are mimicked by OPAA (discussed above). Much like its role in the prolidase activity (see above), the bridging hydroxide, acting as a nucleophile, attacks the phosphorus center of the substrates, followed by the expulsion of the leaving group. In PTE, Asp301 is believed to enhance the OH attack by shuttling its proton to the bulk solvent via His254. PTE Asp301 is homologous to OPAA Glu381, but their action takes place in a different environment; Glu381 is associated with the more exposed MnA metal, whereas Asp301 is linked to the more buried Znα (Figure 5). However, the functions of both His254 in PTE and its equivalent counterpart, His332, in OPAA occur in a similar location (Figure 5), which is also close to the protein surface. The reaction mechanism would require modification in light of our finding, described below, of a difference in the modes of binding of products of OP hydrolysis between OPAA/AMPP and PTE.

Two Different Major Mechanisms for Bridging the Active Site Binuclear Metals by Ligands. Overlapping the binding sites of OPAA loaded with glycolate and reaction product DDP and those of the native AMPP and its complexes with acetate and the inhibitor apstatin (*31*, *37*) (Figure 6; see also Table S4) reveal the following interesting features of the coordinations of the two metal ions by ligands. First and foremost, despite the diversity of ligands (from acetate, the smallest and simplest, to apstatin, the largest and most complicated), only one ligand oxygen atom bridges the two metal ions. This is particularly noteworthy since the ligands have two oxygen atoms that can potentially bridge the two metals. The locations of the oxygen bridging atoms of the ligands coincide with or are very close to the hydroxide or water bridging the two metal ions in native or ligand-free structures [e.g., in AMPP (Figures 4 and 6)]. Second, the second or nonbridging oxygen atom of the glycolate carboxylate (OT2) and DDP phosphate (O2) coordinate the more exposed metal ion (MnA) and further make a hydrogen bond with a His residue (His343) (Figures 2 and 3A,B). Interestingly, this feature, along with the first, has also been observed in the binding of a series of amino acid products and phosphorus-based transition-state analogues to the *E. coli* methionyl aminopeptidase (MetAP) (*49*), which has two Co^{2+} metal centers in the active site very similar to that of OPAA and AMPP. A surprising exception is the binding of the methionine product to *Pyrococcus furiosus* MetAP, which shows one carboxylate oxygen atom interacting with only one of the two metal ions (equivalent to MnA of OPAA/AMPP) and the other oxygen hydrogen bonding with a His residue (*50*). Like the OH of glycolate or the amino group of the isosteric glycine or other Xaa products, the amino group of the bound methionine product interacts with one metal cation (equivalent to MnB). Third, the bridging oxygen atoms are clustered almost to one position, which is very close to that of the bridging hydroxide ion present in the native AMPP structure. Fourth, surprisingly, unlike the two carboxylate oxygens of glycolate, only one oxygen of acetate bound in AMPP participates in metal coordination via the bimetallic bridging mode.

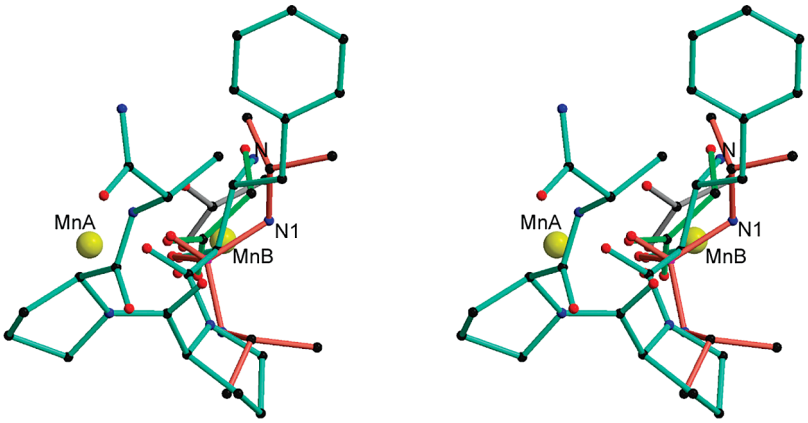

FIGURE 6: Stereo figure of the oxygen atoms of ligands bridging the two Mn^{2+} metal ions in OPAA and AMPP. The ligands bound in OPAA are glycolate (green) and the product inhibitor DDP (salmon), and those in AMPP are acetate (gray) and the inhibitor apstatin (aquamarine). The bridging atoms (colored red) are the carboxylate OT1 atom (glycolate), the phosphate O1 atom (DDP), one carboxylate oxygen (acetate), and a hydroxyl group (apstatin) (see also Table S4). The isolated red sphere represents the bridging OH or water in the native (ligand-free) structure of AMPP (Table S4). One nitrogen of DDP (N1) and apstatin (labeled N) coordinates MnB (see also Figure 3A,B and Table 1). The two Mn^{2+} metals in the overlapped complexes coincide (e.g., see Figure 4), but for the sake of clarity, only MnA and MnB in the OPAA−glycolate structure are shown. The MnA−MnB metal separations in the different ligand-bound structures and the native, ligand-free AMPP are essentially the same (3.3−3.4 Å). The PDB entries of the different structures are listed in Table S4.

These features indicate the variability and pliability of the involvement of particular atoms of ligands in interacting with the bimetallic center. Nevertheless, the one oxygen bridging mechanism is a common feature of ligand binding to OPAA and AMPP.

The one oxygen bridging mechanism in the pita bread structures of OPHs and prolidases and peptidases differs from the mechanism revealed by structural studies of the binding of different products to the bimetallic centers of PTE and other aminohydrolases (e.g., isoaspartyl dipeptidase, dihydroorotase, and D-aminoacylase) with the TIM barrel structural motif. The binding of diethyl phosphate to the PTE, aspartic acid to the dipeptidase, carbamoyl aspartate to the orotase, and acetate to the aminoacylase occurs with two oxygen atoms bridging, in a nearly symmetrical bidentate manner, the two metal ions (see ref *41* and references cited therein). Presumably in this mechanism, one of the oxygen atoms of the product that corresponds to the oxygen of the substrate coordinates the more solvent-exposed metal ion (β), and the other oxygen that originates from the attacking hydroxide ligates the more buried metal ion (α). It is believed that the weakening of the coordination of the bridging or attacking hydroxide to the β-metal ion by the interaction of the substrate with the β-metal ion leads to the coordination of the α-metal ion solely by the oxygen of the product derived from the hydroxide.

What are the possible reasons for the existence of the two distinct types of bridging mechanisms? The one oxygen bridging mechanism may be simpler for binding the products of both peptidase/prolidase and OPH activities since the bridging oxygen, derived from the attacking hydroxide or water molecule, remains in place. It is also possible that this mechanism is more prevalent for binding of products and inhibitors with the additional (or third) polar atom that interacts with the more buried metal ion. This is exemplified by the N1 atom of the product DDP or α-amino group of the Xaa products and the nitrogen (N) of the apstatin inhibitor and the hydroxyl of glycolate, which interacts with MnB metal ion (e.g., see Figures 2, 3A,B, and 6 and Table 1). This interaction could hinder the bridging atom from solely coordinating the MnB ion. On the other hand, the two oxygen bridging mechanisms may be more common for OPHs with OP products, such as those noted above for the enzymes with the TIM barrel architecture, which lack the third metal coordinating atom.

CONCLUSIONS

The principal conclusions that can be drawn from the two crystal structures of OPAA, the native form and its cocrystal with the mipafox inhibitor, are as follows. First, the three-dimensional structure of OPAA is similar to that of a large group of prolidases and peptidases with a bimetallic center located near the surface of a domain with the pita bread architecture. It is most similar to AMPP, as evident by the identical active site geometry for both enzymes. Second, OPAA is unusual in that it is a monomeric protein, whereas AMPP and many others of the group are oligomeric proteins. The oligomeric nature of AMPP is apparently important for its prolidase and OPH activities. Third, unexpectedly, the native OPAA structure revealed the presence of a well-defined nonproteinaceous density in the active site, whose identity could not be conclusively established but is suggestive of a bound glycolate. Fourth, although OPAA was cocrystallized with the inhibitor DDFP (mipafox), the species bound in the crystal structure was attributed to DDP, the product of hydrolysis of DDFP. DDP is held in place by coordination to the binuclear Mn^{2+} atoms and hydrogen bonding and nonpolar interactions with active site residues. The binding of DDP has also revealed three sites, the large and small pockets and the leaving group site, with the latitude of hosting different substituents of ligands, including inhibitors, substrate analogues, and products. The mode of binding of DDFP to OPAA, which is virtually identical to that of DDP, differs from that to AChE and NTE, which occurs by covalent addition through phosphorylation of an active site serine residue and thereby accounts for the severe toxic effect of this and other CWA on the central nervous system. Fifth, in both structures, each Mn^{2+} ion in the active site is coordinated by six atoms of side chains and ligands in a distorted octahedral geometry. Sixth, as prolidases, OPAA and AMPP share very similar features of substrate recognition and catalytic mechanism. The one prominent difference is the role in the tetrameric AMPP of residue(s) of one subunit in catalysis

occurring at an adjacent subunit, which naturally does not occur in the monomeric OPAA. Seventh, although the OPAA structure differs completely from that of the bacterial phosphotriesterase (PTE), remarkably, the geometry of the bimetallic active sites important for OPH activity is conserved in both enzymes. Both enzymes further exhibit very similar OP substrate stereoselectivities and catalytic mechanisms. A major difference is the mode of binding of products between the two enzymes (see below). Eighth, there are two mechanisms for the involvement of oxygen atom(s) of reaction products and inhibitors in bridging the two metal ions in prolidases and OPHs: one involving a single oxygen atom (as seen in OPAA/AMPP and other enzymes with the pita bread architecture) and the other requiring two oxygen atoms (as observed in PTE and other enzymes with the TIM barrel motif). The one-oxygen mechanism is more prevalent for products with three atoms coordinating the two metal ions, whereas the two-oxygen bridging mechanism is more common for products with no more than two oxygen atoms interacting with the bimetallic center.

ACKNOWLEDGMENT

We are grateful to the staff of the Howard Hughes Medical Institute beamline 8.2.1 at the Advanced Light Source, Lawrence Berkeley National Laboratory, for assisting in the collection of diffraction data. We thank Tu-Chen Cheng (BioDefense Team) and Abha Choudhary (Baylor College of Medicine) for technical assistance and advice.

SUPPORTING INFORMATION AVAILABLE

Additional methods and results. This material is available free of charge via the Internet at http://pubs.acs.org.

REFERENCES

1. Mazur, A., and Bodansky, O. (1945) The mechanism of *in vitro* and *in vivo* inhibition of cholinesterase activity by diisopropyl fluorophosphate. *J. Biol. Chem. 163*, 261–276.
2. Mazur, A. (1946) An enzyme in animal tissues capable of hydrolyzing the phosphorus-fluorine bond of alkyl fluorophosphate. *J. Biol. Chem. 164*, 271–286.
3. Hoskins, F. C. G., Kirkish, M. A., and Steinmann, K. E. (1984) Two enzymes for the detoxification of organophosphorus compoounds: Sources, similarities, and significance. *Fundam. Appl. Toxicol. 4*, 165–172.
4. DeFrank, J. J., and Cheng, T.-C. (1991) Purification and properties of an organophosphorus acid anhydrolase from a halophilic bacterial isolate. *J. Bacteriol. 173*, 1938–1943.
5. Cheng, T.-C., Harvey, S. P., and Stroup, A. N. (1993) Purification and properties of a highly active organophosphorus acid anhydrolase from *Alteromonas undina*. *Appl. Environ. Microbiol. 59*, 3138–3140.
6. Cheng, T.-C., Liu, L., Wang, B., DeFrank, J. J., Rastogi, V. K., and Hamilton, A. B. (1997) Nucleotide sequence of a gene encoding an organophosphorus nerve agent degrading enzyme from *Alteromonas haloplanktis*. *J. Ind. Microbiol. Biotechnol. 18*, 49–55.
7. Sutherland, T. D., Horne, I., Weir, K. M., Coppin, C. W., Williams, M. R., Selleck, M., Russell, R. J., and Oakeshott, J. G. (2004) Enzymatic bioremediation: From enzyme discovery to applications. *Clin. Exp. Pharmacol. Physiol. 31*, 817–821.
8. LeJeune, K. E., Dravis, B. C., Yang, F., Hetro, A. D., Doctor, B. P., and Russell, A. J. (1998) Fighting nerve agent chemical weapons with enzyme technology. *Ann. N.Y. Acad. Sci. 864*, 153–170.
9. LeJeune, K. E., Wild, J. R., and Russell, A. J. (1998) Nerve agents degraded by enzymatic foams. *Nature 395*, 27–28.
10. Kropp, T. J., and Richardson, R. J. (2006) Aging of mipafox-inhibited human acetylcholinesterase proceeds by displacement of both isopropylamine groups to yield a phosphate adduct. *Chem. Res. Toxicol. 19*, 334–339.
11. Glynn, P., Read, D. J., Lush, M. J., Li, Y., and Atkins, J. (1999) Molecular cloning of neuropathy target esterase (NTE). *Chem.-Biol. Interact. 119−120*, 513–517.
12. Akassoglou, K., Malester, B., Xu, J., Tessarollo, L., Rosenbluth, J., and Chao, M. V. (2004) Brain-specific deletion of neuropathy target esterase/*swisscheese* results in neurodegeneration. *Proc. Natl. Acad. Sci. U.S.A. 101*, 5075–5080.
13. Kropp, T. J., Glynn, P., and Richardson, R. J. (2004) The mipafox-inhibited catalytic domain of human neuropathy target esterase ages by reversible proton loss. *Biochemistry 43*, 3716–3722.
14. Cheng, T.-C., Harvey, S. P., and Chen, G. L. (1996) Cloning and expression of a gene encoding a bacterial enzyme for decontamination of organophosphorus nerve agents and nucleotide sequence of the enzyme. *Appl. Environ. Microbiol. 62*, 1636–1641.
15. Maher, M. J., Ghosh, M., Grunden, A. M., Menon, A. L., Adams, M. W., Freeman, H. C., and Guss, J. M. (2004) Structure of the prolidase from *Pyrococcus furiosus*. *Biochemistry 43*, 2771–2783.
16. Yaron, A., and Mlynar, D. (1968) Aminopeptidase-P. *Biochem. Biophys. Res. Commun. 32*, 658–663.
17. Kurien, B. T., Patel, N. C., Porter, A. C., D'Souza, A., Miller, D., Matsumoto, H., Wang, H., and Scofield, R. H. (2006) Prolidase deficiency and the biochemical assays used in its diagnosis. *Anal. Biochem. 349*, 165–175.
18. Cheng, T.-C., DeFrank, J. J., and Rastogi, V. K. (1999) *Alteromonas* prolidase for organophosphorus G-agent decontamination. *Chem.-Biol. Interact. 119−120*, 455–462.
19. Leslie, A. (1992) Recent changes to the MOSFLM package for processing film and image plate data, Joint CCP4 + ESF-EAMCB Newsletter on Protein Crystallography, Vol. *26*.
20. Otwinowski, Z., and Minor, W. (1997) Processing of X-ray diffraction data collected in oscillation mode. *Methods Enzymol. 276*, 307–326.
21. Brunger, A. T., Adams, P. D., Clore, G. M., DeLano, W. L., Gros, P., Grosse-Kunstleve, R. W., Jiang, J. S., Kuszewski, J., Nilges, M., Pannu, N. S., Read, R. J., Rice, L. M., Simonson, T., and Warren, G. L. (1998) Crystallography & NMR system: A new software suite for macromolecular structure determination. *Acta Crystallogr. D54*, 905–921.
22. Jones, T. A., Zou, J. Y., Cowan, S. W., and Kjeldgaad, M. (1991) Improved methods for building protein models in electron density maps and the location of errors in these models. *Acta Crystallogr. A47*, 110–119.
23. Sack, J., and Quiocho, F. (1997) CHAIN: A crystallographic modelling program. *Methods Enzymol. 277*, 158–173.
24. Lawskowski, R. A., McArthur, M. W., Moss, D. S., and Thorton, J. M. (1993) PROCHECK: A program to check the stereochemical quality of protein structures. *J. Appl. Crystallogr. 26*, 282–291.
25. Kraulis, P. (1991) MOLSCRIPT: A program to produce both detailed and schematic plots of protein structures. *J. Appl. Crystallogr. 24*, 946–950.
26. Wallace, A. C., Laskowski, R. A., and Thornton, J. M. (1995) LIGPLOT: A program to generate schematic diagrams of protein-ligand interactions. *Protein Eng. 8*, 127–134.
27. Bahadur, R. P., and Zacharias, M. (2008) The interface of protein-protein complexes: Analysis of contacts and prediction interactions. *Cell. Mol. Life Sci. 65*, 1059–1072.
28. Roderick, S. L., and Matthews, B. W. (1993) Structure of the cobalt-dependent methionine aminopeptidase from *Escherichia coli*: A new type of proteolytic enzyme. *Biochemistry 32*, 3907–3912.
29. Carrel, J. C., Carrel, H. L., Erlebacher, J., and Glusker, J. P. (1988) Structural aspects of metal ion-carboxylate interactions. *J. Am. Chem. Soc. 110*, 8651–8656.
30. Christianson, D. W. (1997) Structural chemistry and biology of manganese metalloenzymes. *Prog. Biophys. Mol. Biol. 67*, 217–252.
31. Wilce, M. C., Bond, C. S., Dixon, N. E., Freeman, H. C., Guss, J. M., Lilley, P. E., and Wilce, J. A. (1998) Structure and mechanism of a proline-specific aminopeptidase from *Escherichia coli*. *Proc. Natl. Acad. Sci. U.S.A. 95*, 3472–3477.
32. Levitt, M., and Perutz, M. F. (1988) Aromatic rings act as hydrogen bond acceptors. *J. Mol. Biol. 201*, 751–754.
33. Hoskins, F. C. G. (1985) Inhibition of a soman- and diisopropylphosphorofluorodate (DFP)-detoxifying enzyme by mipafox. *Biochem. Pharmacol. 34*, 2069–2072.
34. Johnson, M. K. (1977) Improved assay of neurotoxic esterase for screening organophosphates for delayed neurotoxicity potential. *Arch. Toxicol. 37*, 113–115.
35. Graham, S. C., and Guss, J. M. (2008) Complexes of mutants of *Escherichia coli* aminopeptidase P and the tripeptide substrate ValProLeu. *Arch. Biochem. Biophys. 469*, 200–208.
36. Zheng, J., Constantine, C. A., Zhao, L., Rastogi, V. K., Cheng, T. C., Defrank, J. J., and Leblanc, R. M. (2005) Molecular interaction between organophosphorus acid anhydrolase and diisopropylfluorophosphate. *Biomacromolecules 6*, 1555–1560.

37. Graham, S. C., Maher, M. J., Simmons, W. H., Freeman, H. C., and Guss, J. M. (2004) Structure of *Escherichia coli* aminopeptidase P in the complex with the inhibitor apstatin. *Acta Crystallogr. D60*, 1770–1779.
38. Graham, S. C., Bond, C. S., Freeman, H. C., and Guss, J. M. (2005) Structural and functional implications of metal ion selection in aminopeptidase P, a metalloprotease with a dinuclear metal center. *Biochemistry 44*, 13820–13836.
39. Graham, S. C., Lilley, P. E., Lee, M., Schaeffer, P. M., Kralicek, A. V., Dixon, N. E., and Guss, J. M. (2006) Kinetic and crystallographic analysis of mutant *Escherichia coli* aminopeptidase P: Insights into substrate recognition and the mechanism of catalysis. *Biochemistry 45*, 964–975.
40. Ghanem, E., and Raushel, F. M. (2005) Detoxification of organophosphate nerve agents by bacterial phosphotriesterase. *Toxicol. Appl. Pharmacol. 207*, S459–S470.
41. Kim, J., Tsai, P.-C., Chen, S.-L., Himo, F., Almo, S. C., and Raushel, F. M. (2008) Structure of diethyl phosphate bound to the binuclear metal center of phosphotriesterase. *Biochemistry 47*, 9497–9504.
42. Aubert, S. D., Li, Y., and Raushel, F. M. (2004) Mechanism for the hydrolysis of organophosphates by the bacterial phosphotriesterase. *Biochemistry 43*, 5707–5715.
43. Hill, C. M., Wu, F., Cheng, T.-C., DeFrank, J. J., and Raushel, F. M. (2000) Substrate and stereochemical specificity of the organophosphorus acid anhydrolase from *Alteronomonas* sp. JD6.5 toward *p*-nitrophenyl phosphotriesters. *Bioorg. Med. Chem. Lett. 10*, 1285–1288.
44. Hill, C. M., Li, W. S., Cheng, T.-C., DeFrank, J. J., and Raushel, F. M. (2001) Stereochemical specificity of organophosphorus acid anhydrolase toward *p*-nitrophenyl analogs of soman and sarin. *Bioorg. Chem. 29*, 27–35.
45. Vanhooke, J. L., Benning, M. M., Raushel, F. M., and Holden, H. M. (1996) Three-dimensional structure of the zinc-containing phosphotriesterase with the bound substrate analog diethyl 4-methylbenzylphosphonate. *Biochemistry 35*, 6020–6025.
46. Lewis, V. E., Donarski, W. J., Wild, J. R., and Raushel, F. M. (1988) Stereoselective detoxification of chiral sarin and soman analogues by phosphotriesterase. *Biochemistry 27*, 1591–1597.
47. Huang, L.-F., Su, B., Jao, S.-C., Liu, K.-T., and Li, W.-S. (2006) Aminopeptidase P mediated detoxification of organophosphonate analogues of sarin: Mechanistic and stereochemical study at the phosphorus atom of the substrate. *ChemBioChem 7*, 506–514.
48. Benning, M. M., Hong, S.-B., Raushel, F. M., and Holden, H. M. (2000) The binding of substrate analogs to phosphotriesterase. *J. Biol. Chem. 275*, 30556–30560.
49. Lowther, T. W., Zhang, Y., Sampson, P. B., Honek, J. F., and Matthews, B. W. (1999) Insights into the mechanism of *Escherichia coli* methionine aminopeptidase from the structure analysis of reaction products and phosphorus-based transition-state analogues. *Biochemistry 38*, 14810–14819.
50. Copik, A. J., Nocek, G. P., Swierczek, S. I., Ruebush, S., Jang, S. B., Meng, L., D'Souza, V. M., Peters, J. W., Bennett, B., and Holz, R. C. (2005) EPR and X-ray crystallographic characterization of the product-bound form of the Mn^{II}-loaded methionyl aminopeptidase from *Pyrococcus furiosus*. *Biochemistry 44*, 121–129.
51. Harding, M. M. (2006) Small revisions to predicted distances around metal sites in proteins. *Acta Crystallogr. D62*, 678–682.